THERMIONIC CONVERSION

Thermionic (TI) energy conversion relies on the emission of electrons by solids heated to a sufficiently high temperature. Thermoelectron emission phenomenon was discovered by Thomas Edison in 1883 and is still known as the *Edison effect.* Herring and Nichols (1) published a review of thermionic emission as early as 1949. The interest in thermionic conversion was resurrected in the mid-1950s, when Hastopoulos (2) published a description of two thermionic converters. The operation of thermionic converters was first demonstrated in the 1950s by P. Marchuk in the USSR (3) and by Houston (4) and Wilson (5) in the United States. Major advances in thermionic technology had been made through the 1950s and 1960s in the USSR, United States, France, Germany, and many other European countries.

In the 1970s and 1980s, funding for the development of thermionic technology in the United States was significantly decreased. Research continued, however, but at a reduced level, to demonstrate the operation of multicell thermionic fuel elements at General Atomic and Los Alamos National Laboratory. Basic research on thermionic conversion also con-

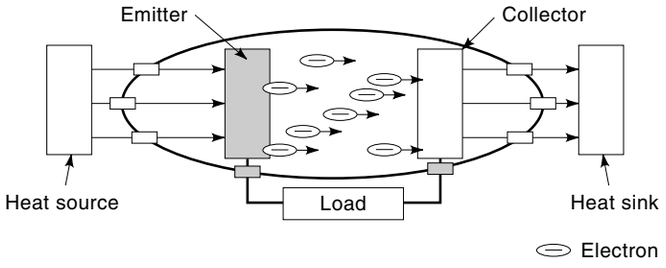

Figure 1. A schematic of a thermionic converter.

tinued by Raser's and Associates, Space Power Inc., Thermacore, Thermoelectron, Inc., and a few universities in the United States. The USSR had continued the development of thermionic technology at a high level, focusing on both multicell and single-cell fuel element concepts for integration into space nuclear reactor power systems. In 1987 and 1988, the USSR announced the successful operation of two thermionic power systems in space for 6 and 12 months, respectively. These power systems, which used in-core multicell thermionic fuel elements (TFEs), became known later in the West as TOPAZ-I. A number of Soviet TOPAZ-II systems, which employed in-core single-cell thermionic fuel elements, had been built and ground tested successfully in late 1970s and in the 1980s, using tungsten electric heaters, instead of nuclear fission, but they had never been deployed in orbit.

Following the end of the Cold War, a joint technology program (1991–1996) was initiated between the United States and Russia and included participation from the United Kingdom and France. The objectives of the program were to (1) perform full-scale tests of a number of TOPAZ-II systems, using tungsten heaters instead of nuclear fuel; (2) explore the use of a TOPAZ-II type power system for future space power and propulsion missions; (3) advance the technology of insulation materials and ceramic-metal brazes; and (4) develop and test advanced high-power density TFEs. This program continued successfully until it was terminated in 1996. The joint tests of the TOPAZ-II system were performed in a special facility that was built for that purpose at the University of New Mexico in Albuquerque.

BACKGROUND

A thermionic converter consists basically of two metal electrodes separated by a small gap of either vacuum or rarefied-vapor plasma. One of the electrodes, maintained at a high temperature is referred to as the *cathode* or *emitter,* and the other, maintained at a lower temperature, is referred to as the *anode* or *collector*. The thermal energy supplied to the emitter from a heat source enables some electrons to escape its surface. These electrons traverse the vacuum or plasma gap, separating the emitter from the collector, and are captured by the collector. They then return to the emitter through an external load, hence producing electrical power (Fig. 1).

The thermodynamic cycle that describes the operation of a thermionic converter resembles that of Carnot, in which thermal energy is ideally supplied to the emitter and removed from the collector at constant temperatures. If joule losses in the electrodes and the leads connecting the converter to the external load are ignored, then the work done by the electrons circulating through the load could be considered adiabatic. The potential difference between the electrodes drives the flow of the electrons through the external load. A converter terminal voltage equals the difference between the electric potentials of the emitter and the collector, minus any internal voltage drop due to the flow of the electrons through the interelectrode gap. Therefore, thermionic converters have a potential for achieving a large fraction of Carnot efficiency. However, this requires the following:

1. Minimizing parasitic thermal losses from the emitter surface (by lateral conduction in the electrodes and leads; by thermal radiation to the collector surface and other structure materials in the gap, such as insulation and metal-ceramic brazes; and by conduction in the plasma-filled gap)
2. Minimizing the voltage drop in the interelectrode gap
3. Minimizing joule losses in the electrodes and the leads to the load
4. Minimizing the collector work function

WORK FUNCTION

Although electrons having an energy within the Fermi conduction band are free to move inside a metal, for them to escape the metal surface they must have sufficient energy to overcome a potential barrier, which is characteristic of the type of the metal. This potential barrier, associated with the electron's positive image charge inside the metal and the uncompensated surface charge, is equal to the difference between the metal's Fermi energy level and the electron's potential in vacuum and is known as the metal's bare work function, φ (typically expressed in electronvolts).

The metal bare work function depends on the crystallographic orientation of the surface (e.g., monocrystalline or polycrystalline) and the type of the metal (6–13). The sorption of rarefied vapor, such as cesium and barium, onto the metal surface lowers its thermionic emission work function, depending on the surface temperature and the vapor pressure of the rarefied vapor (Fig. 2) (14). The sorption of very low-pressure oxygen ($<10^{-2}$ Pa) onto a refractory metal surface has also been shown to increase its bare work function (15). When cesium is sorbed onto such a surface, the oxygenated-cesiated work function of the metal is usually lower than its cesiated work function, resulting in a higher electron emission. The potential difference between the effective work functions of the emitter and the collector also increases, increasing the terminal voltage and the electric power output as well as the conversion efficiency of the converter.

The emission current density, J, is given by the well-known Richardson–Dushman (16–18) equation:

$$J(\mathrm{A/cm^2}) = AT^2 e^{-(e\varphi/kT)} \tag{1}$$

In Eq. (1), e and m_e are the electron charge and mass, respectively, k is the Boltzmann constant, and T is the absolute temperature of the metal surface. For an ideal, isothermal surface, the constant, $A(\mathrm{A/cm^2 \cdot K^2})$, derived theoretically by

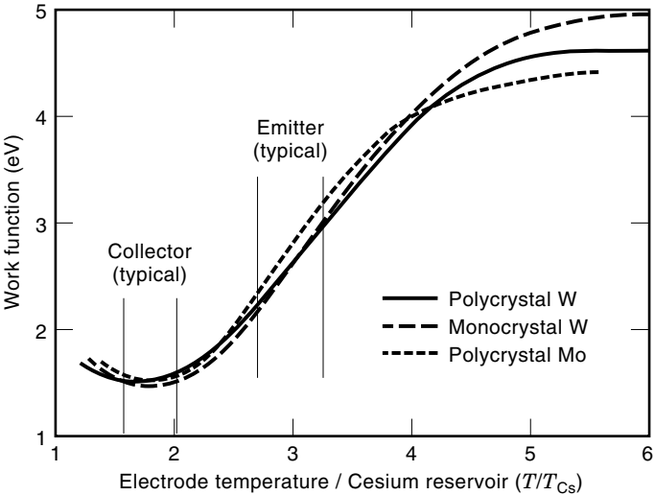

Figure 2. Work functions of refractory metals in cesium (14).

Richardson-Dushman, was given as

$$A = (4\pi e m_e k^2/h^3) = 120.4 \tag{2}$$

In Eq. (2), h is Planck's constant. The actual value of A, however, is determined experimentally and depends on the surface characteristics and the experimental method used and thus could vary slightly from one source to another. Tables 1 (16) and 2 list typical values of the bare work function and the constant, A, for a number of typical electrode materials. As Table 1 indicates, the actual values of A could be much lower than the theoretical value of Richardson–Dushman [Eq. (2)].

All refractory metals, capable of prolonged operation at typical emitter and collector temperatures between 1800 K and 2000 K, and 800 K and 1000 K, respectively, have high bare work functions (in excess of 4 eV) (Tables 1 and 2). The electrode work functions are adjusted during operation by controlling their respective temperatures and the cesium vapor pressure in the interelectrode gap (Fig. 2). When Cs atoms are sorbed onto a refractory metal surface, having a higher bare work function higher than that of Cs (1.89 eV), they are ionized (cesium's first ionization potential, E_i = 3.89 eV), producing a local electric field that reduces the metal's effective work. Since the high sorption energy of cesium and the high bare work of an electrode material result in a low cesiated work function, monocrystal tungsten is the preferred electrode material for thermionic converters (Tables 1 and 2).

Table 1. Bare Work Functions and Emission Constant for Selected Electrode Materials (16)

Electrode Material	Bare Work Function, φ (eV)	A Constant (A/cm^2 · K^2)
Molybdenum (Mo)	4.2	55
Nickel (Ni)	4.61	30
Tantalum (Ta)	4.19	55
Tungsten (W)	4.52	60
	4.54	46
W + Ba	1.6	1.5

Table 2. Bare Work Functions of Typical Electrode Materials

Electrode Material	Bare Work Function, φ (eV)	Electrode Material	Bare Work Function, φ (eV)
W polycrystal	4.54	Nb polycrystal	4.0
W (100)	4.63	Pt polycrystal	5.32
W (110)	5.25	Pt (111)	5.7
W (111)	4.47	Re polycrystal	5.0
Ir polycrystal	5.27	Re (1011)	5.75
Ir (110)	5.42	Ta polycrystal	4.12
Ir (111)	5.76	Ta (100)	4.15
Ir (100)	5.67	Ta (110)	4.8
Mo polycrystal	4.3	W_2C	2.6–4.58
Mo (110)	4.95	ZrC	2.1–4.39
Mo (111)	4.55	Cs	1.8
Ni polycrystal	4.1	Ba	2.2

The collector always operates near the minimum cesiated work function, while the cesiated emitter work function should be significantly higher (Fig. 2), in order to maximize the terminal voltage and the conversion efficiency (7,10).

The emitter temperature and the operating cesium reservoir temperature (or vapor pressure) are, therefore, selected to reduce the effect of the space charge near the emitter and at the same time increase electron emission. For a given emitter temperature, low cesium pressure increases the effective emitter work function and, hence, the terminal voltage but fails to eliminate the space-charge effect, lowering the electron emission and increasing the voltage drop in the gap. The space-charge effect can be eliminated through the combination of using a small interelectrode gap and/or introducing cesium at the proper vapor pressure into the gap. The Cs ions for the plasma in the gap are produced mainly by surface ionization at low vapor pressure and by impact, or volume ionization, at high cesium vapor pressure. The plasma density, n, due to Cs ionization is given by the Saha–Langmuir equation:

$$\frac{n}{n_{tot}} = \frac{g_i}{g_o} e^{\frac{-e(E_i-\varphi)}{kT}} \tag{3}$$

where n and n_{tot} are the plasma density and total density of charged and neutral particles, respectively, and g_i and g_o are statistical weights for ions and atoms, respectively. The ionization of Cs atoms can occur through a single step (Cs + $e^- \rightarrow Cs^+ + 2e^-$) or a multistep (Cs + $e^- \rightarrow$ Cs* + e^-; Cs* + $e^- \rightarrow Cs^+ + 2e^-$) ionization (where Cs* denotes a Cs atom in the excited state). In the case of the impact ionization, the plasma concentration distribution in the interelectrode gap is influenced by the various transport effects (discussed later) as well as the local net rate of ion generation (ionization-recombination rate), $\Gamma(x)$, which can be given as (3)

$$\Gamma(x) = \frac{n_i(x)}{\tau_i}\left[1 - \frac{n_i^2(x)}{n^2(T_e)}\right] \tag{4}$$

where τ_i is the effective ionization time, $n_i(x)$ is the local plasma concentration, and $n(T_e)$ is the equilibrium plasma concentration [Eq. (3)], at T_e, the local electron temperature.

MODES OF OPERATION

This section describes the different types of thermionic converters and the mode of electron discharge in each. The earliest types of converters are those that employ vacuum or quasi-vacuum discharge. Because of the inherently very low emission current, their use is limited to special-purpose applications such as radiation-hard integrated circuits. For electric power conversion applications, however, in which an electric power density of 1 W/cm^2 to 15 W/cm^2 or higher is required, other discharge mode converters are more suitable, such as those that operate in the Knudsen and ignited modes of discharge. The major features of the different discharge mode converters as well as the advantages and limitations of each are discussed in the following subsections.

Vacuum and Quasi-Vacuum Modes of Discharge

The most familiar thermionic converters are those that operate in the vacuum and quasi-vacuum modes of discharge. However, because of their low power density, they are of very limited practical use. Vacuum discharge converters have no Cs in the interelectrode gap, which is kept very small, on the order of 1 μm or less, to avoid the formation of a space charge. In these converters, the discharge current density is typically very small (mA/cm^2). This would require a very large electrode area or operating at very high emitter temperature to achieve a meaningful electric power output ($\leq$mW/cm^2). High-temperature operation in vacuum converters, however, is not possible because it risks closing the gap, due to the thermal expansion of the electrodes, and shorting the converter.

In the quasi-vacuum mode converters, Cs is introduced into the interelectrode gap, but its pressure is kept quite low (a few millitorrs), just enough to adjust the electrodes' work function, as discussed earlier, but not sufficient to neutralize the space charge near the emitter surface. Very little or no surface or impact ionization of cesium takes place in the gap, since the electron mean free path, λ_e, is much larger than the interelectrode gap size, $d(\lambda_e > d)$. Consequently, the space charge forming at the emitter surface repels the emitting electrons, limiting the converter's discharge current. In other words, the space charge increases the effective emission work function by a certain amount, $\Delta\varphi$, that depends on the extent of the space-charge region near the emitter surface. In this type of converter, the emission current can still be calculated using the Richardson-Dushman relation [Eq. (1)], but after accounting for the space-charge effect, as follows:

$$J(\mathrm{A/cm^2}) = AT^2 \exp(\varphi + \Delta\varphi)/kT) \tag{5}$$

Knudsen Mode of Discharge

In Knudsen mode converters, the interelectrode gap size is significantly larger than in vacuum and the quasi-vacuum mode converters. Also, the Cs pressure in the gap is sufficiently high to partially, or completely, neutralize the space charge by the Cs ions generated by surface ionization at the emitter surface. In Knudsen discharge, the Cs pressure is not high enough, however, to produce volume ionization by the collisions of electrons with neutral Cs atoms in the gap (in Knudsen mode $\lambda_e > d$). The condition for a complete space-charge neutralization (i.e., $n_e = n_i$), when operating in Knudsen discharge, can be written as

$$\frac{j_i}{j_e} = \sqrt{\frac{m_e}{m_{Cs}}} \tag{6}$$

where j_e and j_i are the electron and ion currents, respectively, and m_{Cs} is the mass of a Cs atom. The minimum bare work function of the emitter, φ_E^o, required for complete space-charge ionization, is given as

$$\varphi_E^o = \frac{1}{2}E_i + \frac{1}{2}kT_E \ln\left(\frac{2AT_E^2}{en_o}\sqrt{\frac{m_e}{m_{Cs}}}\right) \tag{7}$$

where n_o is the flux of neutral Cs atoms to the emitter and T_E is the emitter temperature. When $j_i > j_e\sqrt{m_e/m_{Cs}}$, there are excess ions and the converter is said to operate in the overcompensated mode. In the undercompensated mode, however, $j_i < j_e\sqrt{m_e/m_{Cs}}$, and the rate of ion generation is not sufficient to neutralize the space charge fully (hence the emission current becomes space-charge limited).

Assuming complete space neutralization (ideal Knudsen mode converter), the relation between the interelectrode voltage and net emission current density, j (the voltampere characteristics) can be readily determined from the following equations:

$$j_E = AT_E^2 e^{-\frac{e\varphi_E}{kT_E}} \quad \text{and} \quad j_C = AT_C^2 e^{-\frac{e(\varphi_E - V)}{kT_c}} \quad \text{for} \quad V \leq \varphi_E - \varphi_C \tag{8a}$$

$$j_E = AT_E^2 e^{-\frac{e(\varphi_C + V)}{kT_E}} \quad \text{and} \quad j_C = AT_C^2 e^{-\frac{e\varphi_C}{kT_C}} \quad \text{for} \quad V > \varphi_E - \varphi_C \tag{8b}$$

and

$$j = j_E - j_C \tag{8c}$$

In these equations, φ_C and T_C are the collector work function and temperature, respectively; and j_E and j_C are the electron emission current densities from the emitter and the collector, respectively.

The voltampere characteristics of an ideal, Knudsen mode converter is shown in Fig. 3. In the saturation region of the voltampere characteristics, all the electrons from the emitter are accelerated in the gap and reach the collector; however, those emitted by the collector are partially repelled back. Only those electrons with energy higher than $(\varphi_E - \varphi_C - V)$ would reach the emitter. In the obstructed region, the situation reverses. According to Eq. [8(c)], the resulting net current equals the difference between the emitter and collector electron currents.

In the Knudsen discharge, a Cs pressure of only a few millitorrs (or tens of pascals) is needed to neutralize the space charge fully. However, such low Cs pressure does not sufficiently lower the emitter work function to produce the high current density required for energy conversion applications. When the Cs pressure is increased, while λ_e is still larger than the gap size, d, losses of electron energy due to collisions with neutral Cs atoms become significant and the operation of the converter transitions to the diffusion mode of discharge.

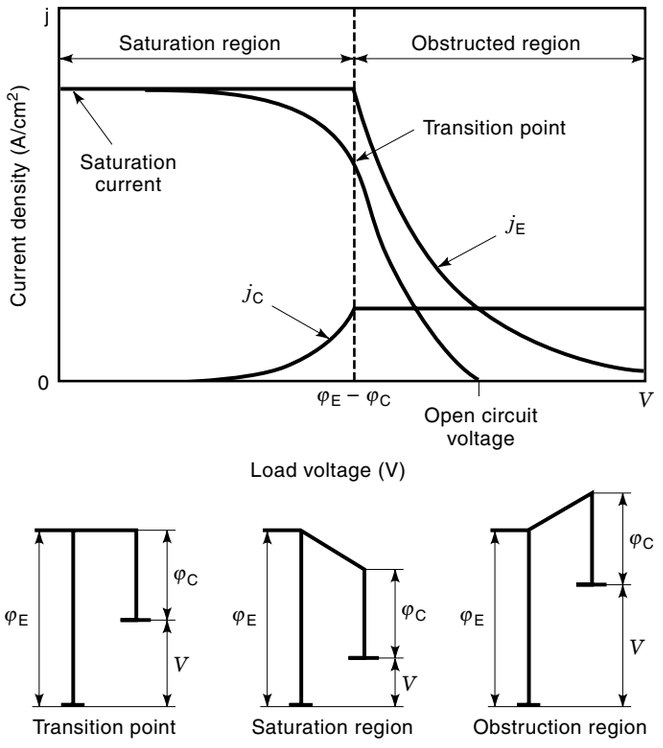

Figure 3. The voltampere characteristics of an ideal, Knudsen mode converter and the corresponding electron motive diagrams.

Diffusion Mode Discharge

The diffusion mode of discharge occurs when the emission electrons undergo frequent collisions with neutral Cs atoms in the gap (diffusion) but the contribution of volume ionization to current discharge is negligible. Hence, the diffusion mode voltampere characteristics and the electron motive diagrams are qualitatively similar to those of the ignited mode. Because of the significant losses of electron energy, diffusion mode discharge is not desirable in thermionic conversion for electric power generation, due to the low conversion efficiency. However, thermionic converters may operate in this mode when Cs pressure and/or load voltage are off optimum and when it is desirable to operate at very high current density.

In diffusion mode discharge, as the load voltage is lowered, the emitted electrons gain more kinetic energy as they are accelerated by the interelectrode voltage drop, ΔV. When their energy becomes sufficiently high to cause volume ionization, the operation mode of the converter transitions to the ignition mode discharge. The ignited mode discharge is characterized by overcompensated plasma in the interelectrode gap, due to the high ionization rate of Cs atoms and the low ion diffusion rate as compared with that of the electrons. The emitter, ΔV_E, and collector, ΔV_C, plasma voltage drops change their sign as compared with the diffusion mode (i.e., the emission electrons are accelerated near the emitter and decelerated near the collector) (Fig. 4).

Ignited Mode of Discharge

This is the operation mode of choice in the state-of-the art thermionic converters for electric power applications. It is characterized by the ion generation in the gap by volume ionization of Cs atom due to the collision with emitted electrons. In this mode of discharge, the interelectrode voltage is low enough and the Cs pressure is high enough that the emitted electrons gain sufficient kinetic energy, as they are accelerated in the sheath near the emitter surface, to cause volume ionization of Cs atoms in the gap.

When the load voltage is slightly lower than the ignition voltage, V_{ign}, the overcompensated plasma in the interelectrode gap does not occupy the entire gap and a small region, with a negative space charge, ΔV^*, exists near the emitter. This space charge is called virtual cathode because the effective emitter work function now becomes $\varphi_E^{eff} = \varphi_E + \Delta V^*$. The corresponding portion of the voltampere characteristics is called the obstructed region [Figs. 4(a) and (b)]. As the converter voltage is reduced further, ΔV^* is also reduced, until the transition point or the "knee" is reached, at which the ion generation is just sufficient to neutralize the space charge near the emitter (i.e., $\Delta V^* = 0$). In the saturation region the plasma throughout the gap is overneutralized and all emitted electrons reach the collector. In addition, the high concentration of positive Cs ions near the emitter creates a strong positive electric field on the emitter surface, increasing the saturation current, due to the *Schottky effect,* above the emission current given by Eq. (1). The voltampere characteristics of an ignited mode converter and the corresponding electron motive diagrams are shown in Fig. 4.

The performance and the plasma behavior in the ignited mode converters are described by the following transport equations for electrons and ions, respectively (3):

$$j_e = -eu_e n_e \frac{dV}{dx} - eD_e \frac{n_e}{dx} - u_e n_e (1 + \beta_e) k \frac{T_e}{dx} \tag{9a}$$

and

$$j_i = -eu_i n_i \frac{dV}{dx} + eD_i \frac{n_e}{dx} + u_i n_i (1 + \beta_i) k \frac{T_e}{dx} - R_i \tag{9b}$$

where β_e and β_i are the electron and ion collision coefficients, and R_i is the friction force due to ion-electron collisions. The corresponding electron and ions continuity equations are

$$\frac{dj_e}{dx} = -\frac{dj_i}{dx} = e\Gamma(x) \tag{10}$$

The equations for the electron energy flux, S_e, and its energy balance are

$$S_e = -j_e \left[\left(\frac{5}{2} + \beta_e \right) \frac{kT_e}{e} + V \right] - \lambda_e \frac{T_e}{dx} \tag{11a}$$

and

$$\frac{dS_e}{dx} = -E_i \Gamma(x) - \Delta S_{rad} - \Delta S_{ei} - \Delta S_{ea} \tag{11b}$$

In these equations, λ_e is the thermal conductivity of electrons, and ΔS_{rad}, ΔS_{ei}, and ΔS_{ea} are the losses of electron energy by radiation and by electron–ion and electron–atom collisions, respectively.

When supplemented by the appropriate boundary conditions, electron energy fluxes to and from plasma at both elec-

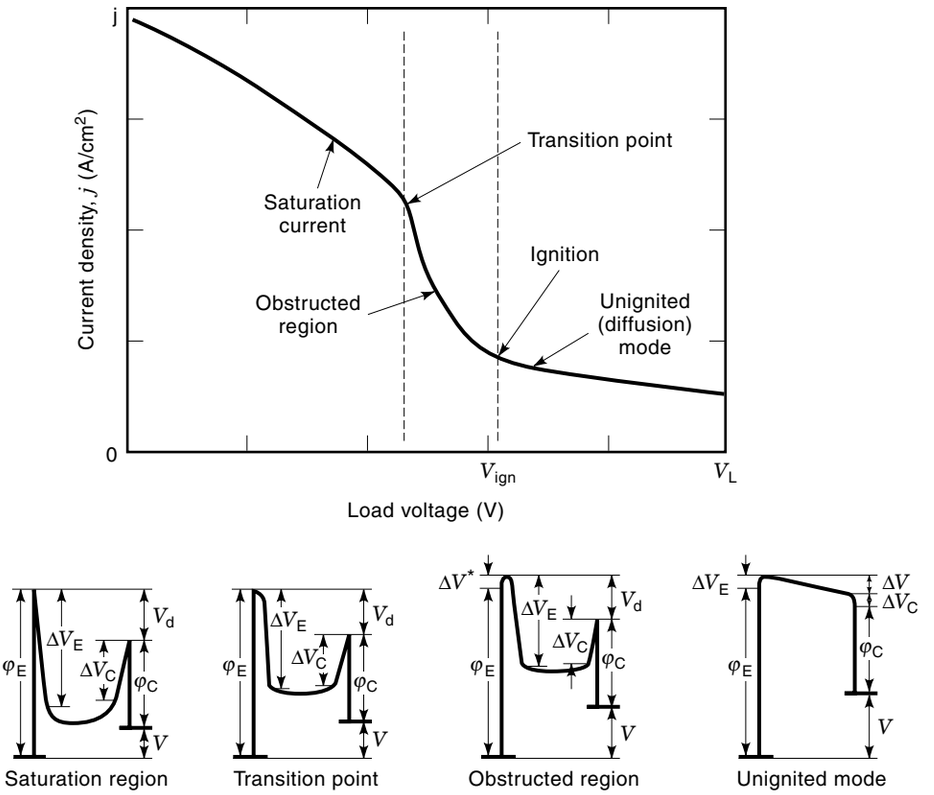

Figure 4. Voltampere characteristics of ignited mode discharge and the corresponding electron motive diagrams.

trode surfaces, Eqs. (9) to (11) could be solved for the distributions of T_e, n, V, j_e, j_i, and S_e across the interelectrode gap, and the net current discharge as functions of the interelectrode voltage.

CONVERSION EFFICIENCY

The total heat flux from the heat source to the emitter surface, q_t, is the sum of several energy quantities:

$$q_{in} = q_{ec} + q_{rad} + q_{Cs} + q_{con} + q_{lead} - 0.5\,q_j \tag{12}$$

In this equation, q_{ec} accounts for the electron cooling of the emitter, q_{rad} accounts for thermal radiation to the cooler collector surface, q_{Cs} accounts for the heat conduction through the Cs-vapor-filled interelectrode gap of the converter, q_{cod} and q_{lead} account for the conduction losses through the electrodes and the leads, respectively, and q_j is the heat generated in the leads by joule effects. The electron cooling heat flux, q_{ec}, is given as

$$q_{ec} = \frac{J}{e}(2kT + e\varphi)T^2 e^{\frac{-e\varphi}{kT}} \tag{13}$$

The thermal radiation heat flux from the emitter to the collector through the interelectrode gap, q_{rad}, is given as

$$q_{rad} = \sigma\epsilon_{eff}(T_E^4 - T_C^4) \tag{14}$$

In this equation, σ is the Stefan–Boltzmann constant (5.67×10^{-12} W/cm$^2 \cdot$ K^4), and ϵ_{eff} is the effective emissivity of the electrodes. The latter depends on the emitter temperature and the electrodes geometric mean temperature, $T_m = (T_E \times T_C)^{0.5}$, and is given as

$$\epsilon_{eff} = (1/\epsilon_E(T_E) + 1/\epsilon_C(T_m) - 1)^{-1} \tag{15}$$

The conduction heat flux through the Cs-vapor-filled interelectrode gap is given also in terms of the emitter T_E, and the collector, T_C, temperatures, using the following empirical relation (17) as

$$q_{cond} = k_{Cs}(T_E - T_C)/\{d + 1.15 \times 10^{-5}(T_E + T_C)/P_{Cs})\} \tag{16}$$

In Eq. (16), d is the interelectrode gap in cm, P_{Cs} is the cesium pressure in the gap in torr [$P_{Cs} = 2.45 \times 10^8\ (T_{Cs})^{-0.5} \exp(-8910/T_{Cs})$], T_{Cs} is the cesium reservoir temperature in kelvin, and k_{Cs} is the thermal conductivity of cesium at the effective temperature, T^*, given as

$$T^* = 2/3\{(T_E^3 - T_C^3)/(T_E - T_C)^2\} \tag{17}$$

For optimized leads, q_{lead} and q_j are given in terms of the conversion efficiency of the converter, as follows (18):

$$q_{lead} = J_o[L(T_E^2 - T_C^2)(2 - \eta/4\eta)]^{0.5} \tag{18a}$$

and

$$q_j = J_o[L(T_E^2 - T_C^2)(\eta/2 - \eta)]^{0.5} \tag{18b}$$

In these equations, L is the Lorenz universal number for metals. It varies from 2.2 to 2.9 $\times 10^{-8}$ V^2/K^2 for pure metals at

273 K and changes very little with temperature above 273 K, increasing typically about 10 to 20% per 1000 K. The voltage drop in a pair of optimized leads can also be expressed in terms of the converter efficiency as (18)

$$V_{\text{lead}} = [L(T_{\text{E}}^2 - T_{\text{C}}^2)(\eta/2 - \eta)]^{0.5} \tag{19}$$

Therefore, the conversion efficiency of a thermionic converter, with optimized leads and negligible lateral heat conduction in the electrodes (isothermal electrodes), can be expressed as

$$\eta = (V - V_{\text{lead}})J_{\text{o}}/q_{\text{in}} \tag{20}$$

where V is the measured terminal voltage of the converter. This equation is solved for the efficiency after substituting for the input heat flux to the emitter, q_{in} [Eqs. (13) to (19)]. The total heat rejection to the heat sink from the collector and the leads, q_{rej}, is given as

$$q_{\text{rej}} = (1 - \eta)q_{\text{in}} \tag{21}$$

TYPES OF THERMIONIC CONVERTERS

Thermionics technology for converting heat to electricity has been under development in the United States, USSR/Russia, France, Germany, and many other countries for more than four decades. These static converters had been developed mostly for space power applications. In such applications, typical emitter (cathode) and collector temperatures are 1850 K to 1900 K and 800 K to 900 K, respectively, and the interelectrode gap is typically 0.1 mm to 0.5 mm wide. The gap is filled with cesium vapor at a pressure as high as 3 torr (400 Pa). The electrodes in thermionic converters (TICs) are usually made of high-temperature refractory metals, such as tungsten, molybdenum, or rhenium. These materials have relatively high bare work functions (4 eV to 5 eV), but their cesiated work functions could be as low as 1.2 eV. The advantages of using TICs in space power and propulsion systems are as follows:

1. There is an absence of moving parts, which potentially increases the converter's operation lifetime, up to 10 years, as well as the system's reliability.
2. The hottest temperature in a TI power system is limited to the emitter (or cathode) assembly (Fig. 5), thus allowing the use of nonrefractory metal, such as stainless steel, as structure material for the coolant loop and the heat rejection radiator.
3. There is low specific mass, since TICs can be operated at very high power density, in excess of 20 W/cm^2. The peak electric power density, however, depends on the electrode temperatures, the type of the converter, the electrode material, the size of the interelectrode gap, and the cesium vapor pressure in the gap. The temperature on the outside of the collector (or anode) assembly (Fig. 5) of about 800 K is low enough to use stainless steel as the structure material but high enough to reject heat by radiation to space at high heat flux, resulting in a lower radiator size and mass.
4. Thermionic converters could be planar or cylindrical, for optimum integration with the heat source (e.g., a nuclear fission reactor or a solar concentrator) [Figs. 5(a) and (b)]. A cylindrical TIC [Fig. 5(b)] could be assembled in single-cell (Fig. 6) and multicell configurations. These configurations are preferred for compact arrangement in a nuclear reactor core, where heat is generated by nuclear fission in the fuel pellets stacked inside the cylindrical emitter tube [Fig. 5(b)]. Cylindrical thermionic elements can also be used outside the nuclear reactor core, where heat is transported to the inside of the emitter surface using high-temperature heat pipes. The heat pipe working fluid could be sodium or lithium, depending on the reactor operation temperature.

   Planar TICs [Fig. 5(a)] can be heated in space using energy from a parabolic solar concentrator. Unlike a nuclear reactor TI power system, a solar TI space system typically has a thermal energy storage unit. Excess thermal energy, while in the sunny portion of the orbit, is stored in a thermal energy storage unit. The stored thermal energy is then recovered and transported to the TICs by the working fluid or by conduction while in the eclipse portion of the flight orbit. Such an energy storage unit adds to the total mass of a TI solar space power system, which is not an issue with terrestrial solar TI power systems.
5. Thermionic converters are inherently radiation hard devices and thus could be used in satellites operating within the Van-Allen ionizing radiation belt, or in power systems for deep space exploration missions.

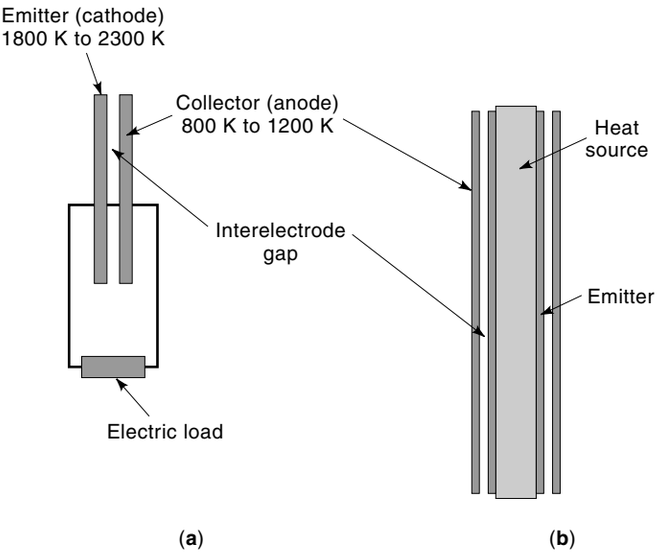

Figure 5. Schematics of a planar and a cylindrical TI converter. (a) Planar TIC. (b) Cylindrical TIC.

Depending on the desired operation conditions, however, there are several types of TICs that have been developed and operated successfully. Some have been tested and operated in a laboratory setup, under well-controlled conditions. A few have been integrated into a nuclear reactor power system (TOPAZ type systems) and were operated in space for up to a year by Russia in 1997. The latter were in-core multicell thermionic fuel elements, cooled by a sodium (23 wt%)-

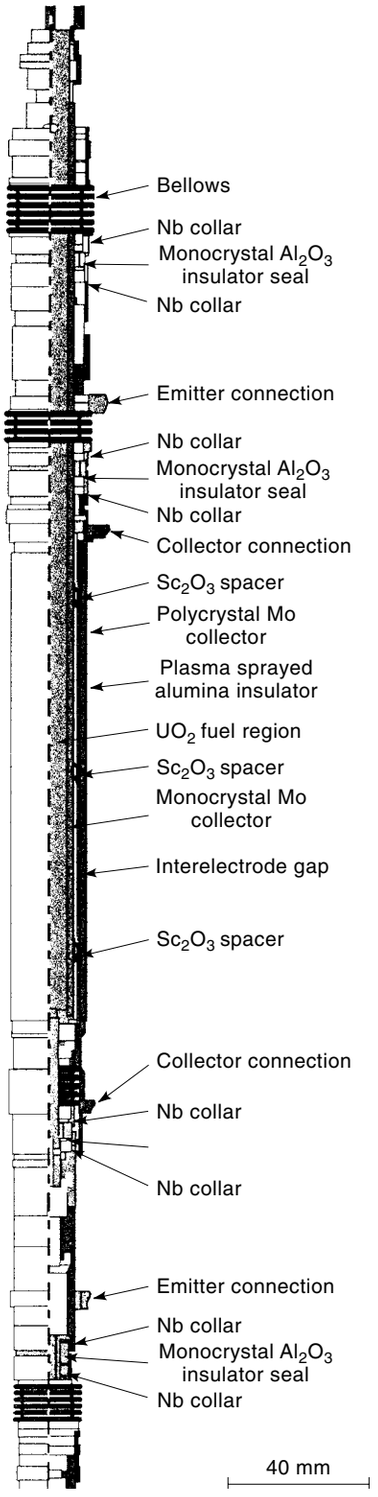

Figure 6. Longitudinal cross section in a fully assembled TOPAZ-I, single-cell thermionic fuel element.

potassium (78 wt%) molten alloy (NaK), which has a freezing temperature of 261 K. Except for the emitter assembly, the rest of the TOPAZ system operates at or below 800 K. Hence, stainless steel has been used as the structure material for the coolant loop. The NaK coolant is circulated through the system using a passive electromagnetic pump, transporting the excess heat from the nuclear reactor core to the system's radiator.

In the following sections, a number of advanced TICs, such as high-temperature cesium TICs, with and without oxygenated electrodes, and cesium–barium high-temperature TICs, are described. These converters have the potential of delivering high conversion efficiency (>15%) and high electric power density (>10 W/cm^2).

In the advanced, high-temperature TICs, the emitter and collector temperature could be as high as 2000 K to 2500 K and 1200 K to 1400 K, respectively. In addition, a brief review and an update on the development of low-temperature planar TICs with grooved electrodes is presented. In these converters, the emitter and collector temperatures range from 1600 K to 1880 K and 800 K to 1200 K. The effect on the TIC performance of introducing inert gases, such as helium and xenon, into the cesium interelectrode gap is also discussed. Finally, the operation principle of microgap TI converters is described.

High-Temperature Cesium Converters

These converters operate at an emitter temperature of 2000 K to 2300 K and a collector temperature of 1000 K to 1200 K and have a relatively small interelectrode gap (<0.5 mm). They have the potential for operating at conversion efficiency of about 12 to 15% and electric power density up to 15 W/cm^2 to 20 W/cm^2. These very high emitter temperatures, however, necessitate using low vapor pressure refractory materials, such as rhenium, as the emitter material to minimize material loss from the emitter surface. The issues of material loss from rhenium (Rh) electrodes at such high emitter temperatures, and in the presence of gaseous traces, such as oxygen, have not yet been investigated. However, the sublimation of Rh would be much lower than tungsten, due to its lower vapor pressure.

High-Temperature Cesium Converters with Oxygenated Electrodes

Many investigations have attempted to increase the conversion efficiency of thermionic converters, beyond the typical 10 to 12% of conventional or common TICs, either by increasing the emitter temperature up to 2100 K to 2300 K and/or introducing tracer amounts of oxygen in the cesium vapor filled interelectrode gap (typically ≤0.5 mm wide). When operating at such high emitter temperatures, however, lifetime issues, such as gradual loss of emitter material and the effects on the TIC performance of the emitter material deposits on the collector surface, should be addressed.

The results of laboratory investigations of thermionic converters with isothermal tungsten emitters have demonstrated that introducing tracer amounts of oxygen or cesium oxides into the interelectrode gap can significantly improve the converter performance (12,19,20). The measured improvements in the conversion efficiency and the electric power density of the TICs were attributed to the following two effects:

1. An increase in the emitter oxygenated bare work function (11,12,21,22) which increases electron emission due to the low oxygenated-cesiated work function of the emitter. Such low emitter work function not only decreases the optimum cesium pressure, corresponding to the maximum TIC electric power output, but also permits the use of a larger interelectrode gap, therefore increasing the converter reliability.
2. A decrease of the minimum work function of the collector surface when covered with tungsten oxide deposits from the emitter surface, which increases the load voltage.

In recent laboratory tests (20), conversion efficiencies of 18% to 22% at power densities up to 15 W/cm^2 (Fig. 7) have been reported. These tests were performed using a planar TIC. Oxygen vapor pressure up to $\sim 8 \times 10^{-6}$ Pa was introduced into the cesium-filled interelectrode gap. The emitter temperature was >1800 K, the collector temperature was ~680 K to 800 K, and the cesium pressure in the interelectrode gap varied from 0.5 torr to 1.5 torr (67 Pa to 200 Pa). The TIC had an emitter made of a CVD (chemical vapor deposition) tungsten coating onto molybdenum and an electropolished molybdenum collector. It has been shown that the introduction of a larger amount of oxygen ($>10^{-6}$ Pa) into the interelectrode gap, however, accelerates the emitter material loss (23,24). It also degrades the converter performance due to the deposit of the oxides of the emitter tungsten on the collector surface (Fig. 8). The degradation in the TIC performance, in this case, can be attributed to several effects:

1. Oxide deposits on the collector surface lower the collector cesiated work function, which increase the load voltage, thus lowering the electric power output and the conversion efficiency.
2. Tungsten oxides increase the thermal losses and electrical current leakage, when deposited onto spacers and insulator surfaces, lowering the electric power output and conversion efficiency.
3. Tungsten oxide deposits could eventually short circuit the electrodes, if chipped off, during thermal cycling or vibrations, and bridge the electrodes (this process is more likely in a small interelectrode gap due to swelling of the thermionic fuel element [TFE] emitter).

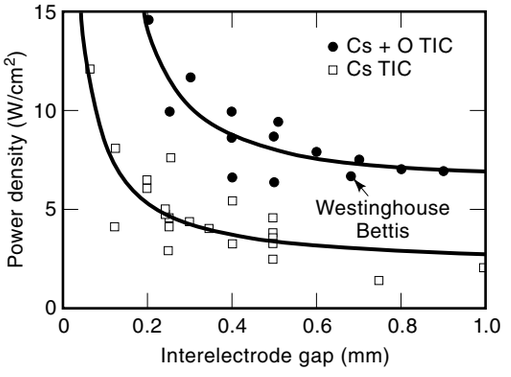

Figure 7. Reported electric power densities for TICs with oxygenated electrodes (20).

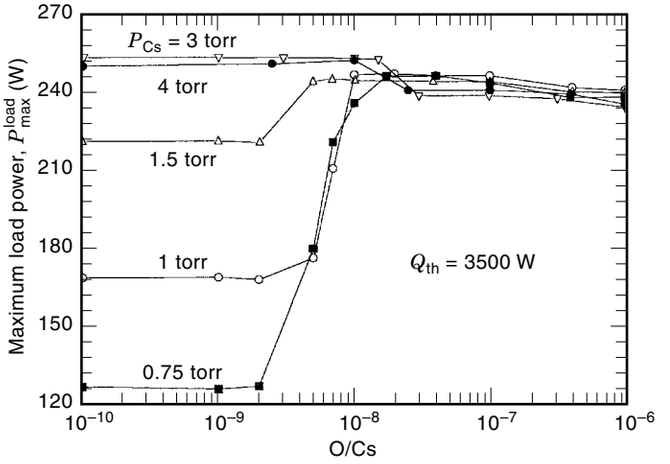

Figure 8. Calculated effect of oxygen on maximum electric power density of a planar converter (23,24).

4. Emitter tungsten loss depletes the emission layer on the emitter surface (typically tungsten), which can eventually result in the base material diffusing to the surface, hence reducing the emitter's bare work function and increasing its cesiated work function.
5. Tungsten oxide deposits on the collector surface increase the effective emissivity of the electrodes, lowering the emitter temperature and, hence, the emission current and conversion efficiency.

The net contribution of all or some of these effects, however, strongly depends on the TIC design and operation conditions. These conditions include the input thermal power, the interelectrode gap size, the type of electrode material, the load resistance, the cesium pressure, and the partial pressures of the gaseous contaminants, such as air, oxygen, water vapor, or carbon dioxide.

Cs–Barium (Ba) High-Temperature Converters

The Cs–Ba converters operate at the same or higher emitter temperatures than the high-temperature Cs converters, but at much lower Cs pressure ($<10^{-2}$ torr versus several torrs in high-temperature Cs converters). In addition to neutralizing the space charge, Cs vapor serves as the transport media for the electrons from the emitter to the collector. The Ba vapor pressure, on order of a millitorr, is sorbed readily onto the emitter surface, lowering its effective emission work function. In other words, Ba in these converters replaces Cs in the high-temperature Cs converters in regulating the work functions of the electrodes. Consequently, it is possible to operate Cs–Ba converters in the Knudsen mode, where scattering losses are almost nil and the maximum electric power output could be derived at a terminal voltage that is equal to the contact potential difference, ($\varphi_{Eo} - \varphi_{co}$).

The optimum current density from the emitter surface, which corresponds to the transition from the unignited to the ignited mode of discharge, J_o, is independent of the type of the emitter material (~1.5 A/cm^2) but increases with the cesium pressure, raised to the one-half power [i.e., $J_o \propto (P_{Cs})^{1/2}$, up to 2×10^{-2} torr] (25). These investigators have demon-

strated experimentally that J_o is almost independent of P_{Cs} in the range from 2×10^{-2} torr to 6×10^{-2} torr. Beyond 6×10^{-2}, however, J_o decreases as the cesium pressure increases because of the scattering of electrons by cesium atoms in the interelectrode gap.

The emitter temperature strongly affects the value of J_o. At $P_{Cs} = 10^{-2}$ torr, J_o almost doubles in value with increasing the emitter temperature in 100 K increments, starting at 1900 K. For example, at T_E = 1900, 2000, and 2100 K, the measured J_o was ~2, 4, and 8 A/cm^2, respectively (25). The optimum emitter work function, φ_{Eo}, also increases as the emitter temperature increases (e.g., φ_{Eo}, = 3.27, 3.65, and 4.04 eV at emitter temperatures, T_E, of 2000, 2500, and 3000 K, respectively).

The only effect the emitter material has on J_o is to change the value of the barium pressure at which J_o occurs. This change is due to the difference in the sorption energies of the barium atoms onto the different electrode materials; the higher the sorption energy of barium, the lower is the optimum barium pressure. For example, because the sorption energy of barium onto tantalum (Ta) is higher than onto tungsten (W), the optimum barium pressure for the former ($\sim 4 \times 10^{-2}$ torr) is higher than that for the latter ($\sim 1.6 \times 10^{-2}$ torr).

In Cs–Ba converters, the optimum P_{Cs} depends on the size of the interelectrode gap. Experimental data have shown that for a gap size of 1.0 and 0.1 mm, the optimum P_{Cs} was 10^{-2} torr and 10^{-1} torr, receptively (26). For these gap sizes and collector temperatures of 1250 K to 1350 K, the optimum collector work function, φ_{co}, was found to be 2.3 eV. This collector work function corresponds to the maximum electric power density of the Cs–Ba converter. The maximum electric power and the corresponding conversion efficiency increased almost exponentially with the emitter temperature, particularly in the range from 2000 K to 2300 K. The maximum power density and conversion efficiency also increased with increasing the optimum cesium pressure. Experimental data have shown that at P_{Cs} of 10^{-2} torr, when the optimum gap size was 1.0 mm, the maximum power density increased from ~1.0 W/cm^2 to ~12 W/cm^2, as the emitter temperature increased from 1900 K to 2300 K, respectively. When the gap size was reduced by an order of magnitude to 0.1 mm (corresponding optimum P_{Cs} = 0.1 torr), the maximum power density was significantly higher, increasing from ~2.3 W/cm^2 to 30 W/cm^2, as the emitter temperature increased from 1900 K to 2300 K, respectively.

The optimum emitter and collector temperatures for the Cs–Ba converters are about 300 K to 400 K higher than those in high temperature Cs converters. These high electrode temperatures make it possible to achieve a conversion efficiency that could be as high as 60% of Carnot, at the same emitter (hot) and collector (cold) temperatures. After accounting for radiation and conduction losses in the gap, the calculated conversion efficiency ranges form 18 to 25% for T_E of 2300 K (25,27). Ender et al. (28) have reported electric power densities up to 15 W/cm^2 (Fig. 9).

Due to the very high emitter temperatures, Cs–Ba converters suffer from the same limitations on their operation lifetime (less than three years), as high-temperature cesium converters discussed earlier, due to the rapid loss of emitter material (28). The operation lifetime of Cs–Ba converters is also limited by finding an appropriate insulation material that is compatible with both Ba and Cs vapor at such high

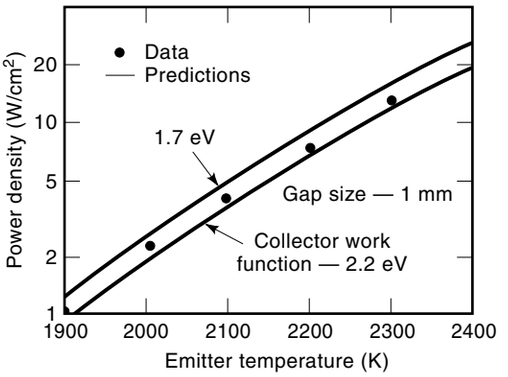

Figure 9. Electric power densities versus emitter temperature for Cs–Ba thermionic converters (28).

temperatures. Also, since Cs–Ba converters operate at a very high electric power density (Fig. 8), large ohmic losses occur in the converter leads and electrodes. To reduce these losses, only planar electrodes, with a relatively small surface area (<10 cm^2), could be used. While planar electrodes are suitable for use in conjunction with solar concentrators, either in space or terrestrial applications (28) and may be used in topping cycles in fossil power plants, they are unsuitable for use with a nuclear reactor heat source.

Grooved Electrodes, Low-Temperature Converters

When a TI converter is operated in the ignited mode of discharge, increasing the cesium pressure increases the electric power output up to a point beyond which scattering losses cause the electric power output to decrease. The optimum cesium pressure, corresponding to the peak electric power, depends on the type of the electrode material and temperatures. For a given cesium pressure, raising the emitter temperature or lowering collector temperature increases the emission current and the potential differential across the external load. The temperature of the collector, however, should not be lower than that corresponding to the minimum cesiated work function of the selected collector material.

On the other hand, increasing the emitter temperature increases the material loss from its surface, by sublimation and formation of volatile oxides, when oxygen pressure in the gap $>10^{-8}$ torr (23,24,29–31). High emitter temperatures also impose a challenge to the integrity of the insulation material and the metal-ceramic brazes in the converter, hence shortening its performance lifetime. Furthermore, increasing the emitter temperature increases the optimum cesium pressure, which results in a high back emission from the collector, lowering the converter's dielectric strength.

Recently, there has been growing interest in developing low-temperature Cs converters for terrestrial applications, such as in topping cycles of fossil electric power plants or diesel-fired engines. In these applications, the source temperature could be several hundred degrees lower than in high-temperature Cs converters (1600 K to 1800 K). A practical approach to enhance the performance of these lower-temperature thermionic converters is to use grooved electrodes. When grooved electrodes converters operate in the so-called hybrid

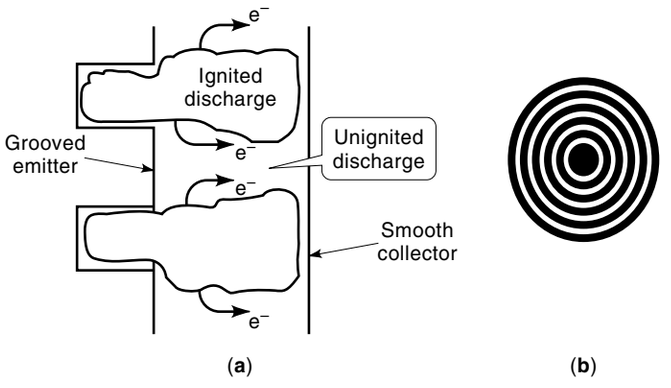

Figure 10. Low-temperature cesium converters with macrogrooved emitter. (a) Hybrid operation in a TIC having a macrogrooved emitter. (b) Macrogrooved emitter design (32).

mode [Fig. 10(a)], the discharge breakdown, or ignition, in the grooves occurs at low cesium pressure and provides

1. electrons for cesium ionization in the nongrooved portion of the emitter surface, which operates in the diffusion mode
2. Cesium ions, which diffuse from the grooved to the nongrooved portion of the emitter surface, contributing to the neutralization of the space charge, hence lowering the optimum cesium pressure (32,33) [Fig. 10(a)].

Several experiments have been performed using electrodes with macro- and microgrooved electrodes for a wide range of electrode temperatures, cesium pressures, and interelectrode gap sizes, with mixed results (34–38). In general, TI converters with grooved electrodes have performed better than those with smooth electrodes (23,24). The best performance has been reported for emitter temperatures of 1700 K to 1750 K, showing an increase of 25% to 50% in the conversion efficiency and the electric power density (Fig. 11). However, due to the lack of systematic studies using the same experimental

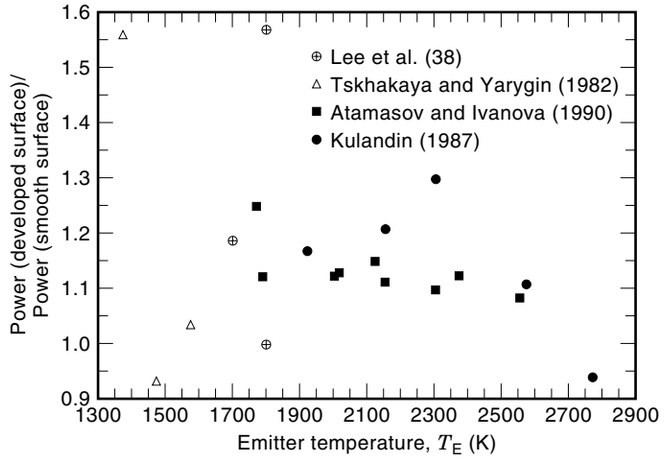

Figure 11. Comparison of electric power of grooved and smooth electrode converters (39).

setup and procedures, reported results were inconclusive and sometimes contradictory (39).

Shimada (34,35) had tested a thermionic converter with molybdenum (Mo) emitter that had 0.5 mm square longitudinal grooves, with a 1.0 mm separation. The nongrooved portion of the emitter was coated with rhenium, which has a high bare work function and hence lower cesiated work function than Mo. Shimada reported a 300% increase in electric power output, compared to a smooth electrode converter. Tskhakaya et al. (36) tested a converter with a smooth zirconium oxide collector and an Mo emitter that had grooves similar to that of Shimada's, but the tops were coated with platinum. They compared the electric power output with that for a converter that had a smooth platinum emitter and zirconium oxide collector.

Although the performance of the former was better than the latter, Tskhakaya et al. (36) were unable to duplicate the large increase in electric power output reported by Shimada (34,35). Their optical observations of plasma discharge confirmed that, while the grooves supplied ions to the rest of the gap [Fig. 10(a)], the converter did operate in the hybrid mode described by Shimada.

Tskhakaya et al. (36) results also showed that the optimum gap size for their grooved emitter converter (1.6 mm) was higher than that for a smooth electrode converter (1.0 mm). They have also tested a converter with a grooved emitter and a zirconium oxide collector that had the same grooves as the emitter. In these experiments, the collector's grooves were laid in the perpendicular direction to the emitter's grooves.

Atamasov et al. (37) had tested a converter consisting of a single-crystal, smooth tungsten emitter and five microgrooved collectors in the same test device. The interelectrode gap was 0.35 mm wide. They applied an axial magnetic field to eliminate edge effects and electron scattering between various collectors. The longitudinal grooves in all collectors were 0.1 mm wide and 0.15 mm apart but had different depths of 0.1 mm to 0.5 mm. The measured peak electric power was 20% to 60% higher than with a smooth collector and occurred at 0.1 V to 0.2 V higher terminal voltage. Recently, Lee et al. (38) performed a series of experiments with four electrode combinations, namely (1) smooth electrodes, (2) microgrooved emitter and smooth collector, (3) smooth emitter and microgrooved collector, and (4) microgrooved electrodes. The emitter grooves were 0.075 mm wide, 0.25 mm deep, and 0.075 mm apart, while the collector grooves were 0.1 mm wide, 0.25 mm deep, and 0.125 mm apart. The emitter was made of tungsten chloride, the collector material was niobium, and the size of the interelectrode gap varied from 0.125 mm to 0.5 mm. Their results showed a 0.1 V increase in the output voltage of converter (1), a small increase in the electric power output and a 50% increase in the emission current density of converter (3), and no discernible difference in the performance of converter (4) compared to the converter (1).

Recently, El-Genk and Luke (32) performed experiments to characterize the performance of developed electrodes TI converters [Fig. 10(b)], as a function of the cesium pressure, (P_{Cs} = 10 Pa to 240 Pa). They tested three configurations: (1) smooth electrodes converter, (2) grooved emitter converter, and (3) grooved collector converter, at the same cesium pressures and interelectrode gap size (1.5 mm). Results showed that the grooved emitter converter gave higher electric power

output than the smooth electrode converter at low Cs pressure, similar to previous results of Atamasov et al. (37) and Lee et al. (38). Furthermore, the peak electric power output for the former (0.4 W/cm^2) occurred at a lower cesium pressure (120 Pa) than the peak electric power for the latter (0.31 W/cm^2 at 150 Pa).

This reduction in the cesium pressure at the peak electric power of the grooved emitter converter was apparently due to the space-charge neutralization at the emitter surface by diffusing ions from the grooves to the tops portion of emitter surface [Fig. 10(b)]. The electric power output of the grooved emitter converter was more than a factor of 2 higher than that of the smooth electrode converter at P_{Cs} = 57 Pa, decreasing to only 5% at 240 Pa (32). The peak electric power for the grooved emitter converter (0.4 W/cm^2) occurred at P_{Cs} = 120 Pa, while that of the smooth electrodes converter (0.325 W/cm^2) occurred at a higher P_{Cs} = 150 Pa.

They also reported that at cesium pressure less than 110 Pa, the electric power output of the grooved collector converter was also higher than that of the smooth electrode converter, but lower than that for the grooved emitter converter (32). At higher cesium pressure, the electric power of the grooved collector converter was the highest, and peaked at the same cesium pressure as the smooth electrodes converter (150 Pa). The electric power output of the grooved collector converter was 1.4 times that of the smooth electrodes converter, which is the same as the increase in the grooved collector surface area. Since the use of a grooved collector does not affect space-charge neutralization at the emitter surface, the electric power output for the grooved collector converter peaked at the same cesium pressure as the smooth electrode converter.

For emitter and collector temperatures of 1573 K and 1073 K, respectively, the conversion efficiency of the grooved collector converter was more than 70% and 20% higher than that for the smooth electrodes converter at P_{Cs} of 60 Pa and 240 Pa, respectively (32). The conversion efficiency of the grooved emitter converter was almost twice that of the smooth electrode converter at P_{Cs} = 60 Pa, but the same at 240 Pa. The efficiency of the smooth electrode converter was significantly lower than those of the other two converters at low cesium pressure, but approached that of the converter with a grooved emitter and a grooved collector as P_{Cs} increased. The peak conversion efficiency of 5.8% for the converter with a grooved collector occurred at P_{Cs} = ~140 Pa, at which the conversion efficiencies of the grooved emitter and smooth electrodes converters were 5.16% and 4.9%, respectively. The peak conversion efficiency of the grooved emitter converter (5.22%, which represents 16.4% of Carnot) occurred at a lower cesium pressure (110 Pa) than the smooth electrode and the grooved collector converters (32).

El-Genk and Momozaki (1998) have continued the work of El-Genk and Luke (32), but at higher electrode temperatures and P_{Cs} and smaller interelectrode gap size (0.5 mm). They varied the emitter temperature from 1573 K to 1773 K and P_{Cs} from 50 Pa to 500 Pa. The collector temperatures were 1073 K and 1173 K. A peak electric power density of 1.2 W/cm^2 and a peak conversion efficiency of ~8.8% were achieved at a relatively low emitter temperature of 1773 K and a high collector temperature of 1173 K. This peak conversion efficiency represents ~24.5% of Carnot, at the same emitter and collector temperatures. To obtain the same fraction of Carnot, a Cs–Ba or a high-temperature cesium converter, in which the collector and emitter temperatures are 1200 K and 2500 K, respectively, would have to deliver a conversion efficiency of 12.7%. Similarly, a conventional thermionic converter operating at an emitter temperature of 1900 K and a collector temperature of 800 K would have to deliver a conversion efficiency of ~14.2%, to realize the same fraction of Carnot (24.5%).

The results of El-Genk and Momozaki (33) have also shown that lowering the collector temperature to 1073 K significantly increased the electric power density and conversion efficiency. At emitter and collector temperatures of 1573 K and 1073 K, respectively, the measured peak electric power density and peak conversion efficiency were more than 20% and 12% higher, respectively, than those for identical converter with a larger gap of 1.5 mm. Results suggested that lowering the collector temperature to about 800 K could further enhance the performance of grooved electrodes converters, in terms of both higher efficiency and electric power density. Further research on grooved electrode converters could be rewarded handsomely by opening a broad range of potential application for commercial electric power generation.

Effect of Inert Gases on the Performance of Cesium TICs

There was a lot of interest in the 1960s and 1970s in investigating the effect of inert gases, such as helium and xenon, on the performance of Cs converters. Inert gases affect the transport and distribution of Cs ions in the interelectrode gap. While chemically inert, they have a low scattering cross section for slow electrons, and their high ionization potential impedes surface ionization as well as ion diffusion, but not electron diffusion. Also, due to the very large temperature gradient in the gap (~2000 K/mm), the relative diffusion of the inert gases and Cs ions could alter the Cs ion density at the emitter by forcing them to diffuse into the colder region of the gap, hence altering the saturation emission current. The results of earlier work have been contradictory, with some showing an increase in the electron current (or a decrease in internal voltage drop) and others showing the opposite effect.

Kaplan and Merzenich (40) and Bekmukhambetov et al. (41) reported that the addition of xenon or krypton (up to ~60 torr) to cesium in the interelectrode gap has increased the electron current by as much as 15% to 20%. They attributed this increase in the electron current to a reduction in the internal voltage drop required for volume ionization. Kondrat'ev et al. (42) have shown that increasing the xenon pressure in the interelectrode gap from 3 torr to 10 torr increased electron current; however, a further increase in xenon pressure caused the electron current to decrease. They attributed the results to two competing mechanisms: (1) higher ion density, since xenon tends to impede the diffusion of cesium ions out of the interelectrode gap; and (2) increased electron scattering due to the presence of high-pressure xenon.

Kaplan and Merzenich (40) reported a decrease in the electron current when neon was added to the cesium in the interelectrode gap. Rufeh and Kitrilakis (43) reported a systematic reduction in the electron current (or increase in internal voltage drop) as the pressure of argon gas in the interelectrode gap was increased from 0 torr to 100 torr. Gverdtsiteli et al.

(44) showed a significant increase in electron current, however, in the presence of argon in the interelectrode gap.

Rufeh and Lieb (45) performed a series of experiments using a thermionic converter that had a rhenium emitter and a molybdenum collector, and they varied the interelectrode gap from 0 mm to 2.5 mm. The emitter temperature was 1800 K, the cesium pressure was about 1 torr, and the inert gas pressure was varied in small steps from 0 torr to 200 torr. Unlike some of the earlier work, they reported a consistent decrease in the electron current (or increase in the internal voltage drop) when inert gases (xenon, krypton, or argon) were introduced into the interelectrode gap. The decrease in the electron current increased as the pressure of the inert gas increased. Rufeh and Lieb (45) attributed the reported increase in electron current by earlier investigators to the presence of impurities, such as oxygen, in the inert gases. At very low cesium pressure, on the order of 10^{-2} torr, an increase in the output voltage or electron current was reported when inert gases were introduced into the interelectrode gap (44,46).

Most recently, Tschersich and Niekizch (47) have investigated the effect of xenon on the voltage drop in the interelectrode gap of a cesium converter. They performed experiments using a variable-spacing converter that had a polycrystalline tantalum emitter and a polycrystalline niobium collector. They used a method similar to that of Rufeh and Lieb (45) to ensure that oxygen impurities were not introduced with the xenon gas. The values of $P_{Cs}d$, where d is the size of the interelectrode gap, were 4×10^{-3} torr-cm to 5×10^{-2} torr-cm (P_{Cs} from 0.13 torr to 1.84 torr) and the pressure of xenon was increased from 0 torr to 80 torr. Their results showed a remarkable reduction in the internal voltage drop when the value of $P_{Cs}d$, was below the optimum value ($\sim 5 \times 10^{-2}$ torr-cm). For example, at $P_{Cs}d$ of 2.6×10^{-3} torr-mm (d = 0.2 mm and P_{Cs} = 0.13 torr), increasing the xenon pressure from 0 torr to 50 torr decreased the internal voltage drop from 1.38 V to 0.8 V (a 0.58 V decrease). At the same cesium pressure, when the gap size was increased five times to 1.0 mm, the internal voltage drop decreased from ~0.715 V to a minimum of ~0.55 V (a decrease of 0.17 V) as xenon pressure increased from 0 torr to 20 torr).

Near the optimum $P_{Cs}d$, the change in internal voltage drop as well as its minimum value, due to the presence of xenon, was relatively small and negligible, respectively. Beyond the optimum $P_{Cs}d$, there was no effect on the internal voltage drop due to the addition of xenon. The lowest voltage drop measured in the absence of xenon was 0.55 V at a $P_{Cs}d$ of 2×10^{-2} torr. The results of Tschersich and Niekizch (47) have confirmed earlier results that introducing inert gasses increases the electron current (or reduce the internal voltage drop) in Cs converters. These results, however, are in disagreement with those of Rufeh and Lieb (45).

In summary, it may be argued that the introduction of inert gases in cesium converters would improve their performance (i.e., increase the electron current or reduce the internal voltage drop) at low cesium pressure, due to the retention of Cs ions by inert gases and negligible scattering losses. At high cesium pressure, there should be no effect if scattering losses are compensated for by the retention of Cs ions. Hence, the introduction of inert gases would improve the performance of Cs converters due to two effects: (1) an increase in the plasma density and enhanced plasma distribution in the gap, and (2) a change in the potential distribution, resulting in a decrease in the internal voltage drop (or increase in the electron current). These results suggest that low electrode temperature Cs converters, such as those with grooved electrodes, could benefit greatly from the addition of inert gases, such as xenon. Since the optimum cesium pressure in these converters would be lower than in conventional and high-temperature Cs converters, the benefit of adding inert gases in the interelectrode gap could be significant, particularly at low-collector temperatures (600 K to 1000 K).

Microgap Converters

Quasi-vacuum and Knudsen mode converters have long been perceived as of very little promise because of the difficulty with maintaining an interelectrode gap size on the order of few microns. However, recent advancements in microelectronics, precise machining, monocrystalline material fabrication, and other manufacturing technologies have made it possible to develop microgap converters. The operation of laboratory-scale microgap converters, with 4 μm to 10 μm interelectrode gap, has been demonstrated successfully at Space Power Inc. by Fitzpatrick et al. (47a) and at the Russian Institute Luch by Nikolaev et al. (1996). The test converters had monocrystalline electrodes to achieve high thermionic performance and provide dimensional stability. During operation, the electrodes are separated by a microsized gap due to the thermal expansion of ceramic spacers recessed in the collector (Fig. 12). An applied helium gas pressure on the collector assembly provided precise control of the interelectrode gap size and minimized parasitic heat losses.

Stable operation of these microgap converters has been demonstrated for hundreds of hours. Ways enhance the performance of these converters in the future include the following:

1. Using monocrystalline emitters, with built-in heat pipes, to maintain uniform electrode temperature, thus preventing structural distortion
2. Implementing active and precise control of the gap size using piezoelectric transducers (47b)
3. Using highly reflective coatings for the collector surface, maintaining high emitter temperature and hence high electron emission

Because the space charge in a Knudsen mode thermionic converter is at least partially compensated for by the Cs ions generated at the emitter surface, the gap size, emitter temperature, and emission current can be significantly increased with very little loss of the electron energy. Typical Knudsen mode microgap converters have an interelectrode gap that is about 20 μm and are operated at emitter temperatures of

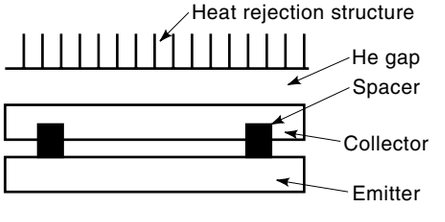

Figure 12. A schematic of a microgap converter.

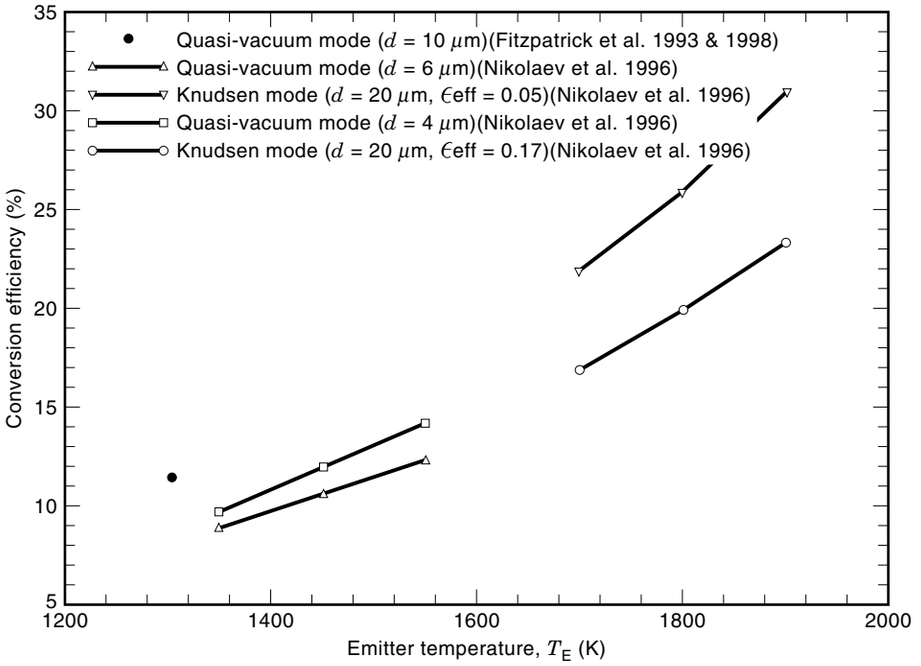

Figure 13. Calculated efficiencies of quasi-vacuum and Knudsen mode microgap converters.

1700 K to 1900 K. At the higher emitter temperatures, however, radiation heat transfer becomes significant, reducing the fraction used for electron emission and resulting in a lower efficiency and electric power density. As delineated in Fig. 13, using a thin, highly reflective (ϵ = 0.05) copper or silver coating of the collector surface is expected to increase the converter efficiency into the 25% to 30% range.

ENGINEERING ASPECTS OF THERMIONIC CONVERSION

The electrode and structural and insulator materials used in thermionic converters need to satisfy strict and sometimes contradictory requirements. For example, the emitter material should possess the following properties:

1. *High bare work function,* to provide low cesiated work function and/or efficient surface ionization
2. *Stable mechanical and surface properties,* to minimize the loss rate of emitter material when operating at high temperatures and in cesium vapor
3. *Low emissivity,* to minimize thermal energy transport to the collector by thermal radiation, increasing electron emission and achieving high conversion efficiency
4. *High electric conductivity but low thermal conductivity,* to minimize joule losses and axial heat conduction, respectively, in the electrodes
5. *Structural strength at high temperatures,* which favors using monocrystalline instead of polycrystalline emitter material. The former also has a higher bare work function than the latter.

The high-temperature emitter materials that satisfy these requirements are therefore limited to tungsten (W), molybdenum (Mo), tantalum (Ta), and rhenium (Rh).

The collector material should have a cesiated work function that is as low as possible at the operating collector temperature and at the cesium vapor pressure in the interelectrode gap to maximize the load voltage. Low emissivity (or high reflectivity) collector is also important, since it directly affects the emitter temperature through the thermal radiation transport between electrodes. Because the collector operates at a relatively low temperature (800 K to 900 K), material loss is of no consequence, but it is important that the collector material remain chemically stable in cesium vapor. The collector material should have a high electric conductivity, to minimize joule losses, and high thermal conductivity, to ensure uniform electrode temperature. The electrodes, however, should be thermally insulated at their edges to minimize thermal losses. In addition to the emitter materials mentioned earlier, other low work function materials, such as Nb, LaB_6, Ba, or Zr oxides, Ni, and even stainless steel, could be used for the collector.

Other important structural components of a thermionic converter are the interelectrode gap spacers and electric insulators, which are usually manufactured of ceramic material that should satisfy the following requirements:

1. Chemical and mechanical stability at operation temperatures and in a cesium environment
2. Linear thermal expansion coefficients similar to other materials used in the converter
3. Low electric and thermal conductivities
4. Low release rate of volatile and gases during operation, to avoid contaminating the cesium vapor in the interelectrode gap
5. High fracture strength in order to withstand thermal cycling and vibrations
6. Good chemical compatibility with emitter and collector materials

Table 3. Causes of Failure and Performance Degradation of TFEs

Cause	Open Circuit	Short Circuit	Degradation
Emitter:			
Change in position, emission coating		+	
Separation			
Damage or deformation		+	
Loss of vacuum tightness, release of fission products			+
Contamination and mass transfer		+	+
Interelectrode gap:			
Lack of cesium	+		+
Penetration of contaminants (from outside or from nuclear fuel)			+
Increase in heat losses			+
Spaces:			
Destruction or damage		+	
Decrease of contact thermal resistance			+
Deposition of conducting layers		+	+
Collector assembly:			
Deposition of contaminants and reaction products			+
Change of cooling conditions			+
Increase in thermal resistance deformation		+	+
Insulation failure		+	+
Emitter-collector commutation:			
Destruction		+	
Cross-section reduction			+

The most commonly used ceramic materials in TI converters are oxides of Al, Be, Zr, Mg, Th, and Sc.

Lifetime and Performance Degradation

Cylindrical (TFE) and planar thermionic converters may experience gradual degradation in performance due to changes in the operation and material conditions of the converter or at the system level. Internal causes of performance degradation are (1) changes in the work function and the effective emissivity of the electrodes; (2) presence of gaseous contaminants in the interelectrode gap; (3) mass transport of emitter material to the collector surface; and (4) changes in the electrode temperatures. Examples of system level causes of performance change are (1) improper operation or a failure of the cesium supply system and the introduction of gaseous contaminants or ambient air into the interelectrode gap; (2) changes in heat rejection, increasing the coolant and the collector temperatures; and (3) a loss of vacuum tightness.

Generally, there are two types of a TFE or thermionic converter failures: open and short circuit. In an open circuit failure, the internal electrical resistance of the converter rapidly increases as the voltage and current on the external load approach zero. For TFEs connected in series to a constant load, a short circuit in one of the TFEs would cause a reduction in the load voltage and current. Also, the slope of the static (constant power) voltampere characteristics will increase. While both open circuit and short circuit failures in a TFE lead to abrupt changes in the voltampere characteristics, gradual changes in the TFE performance cause a slow change in the voltampere characteristics. Table 3 provides a list of various causes of failure and performance change in electrically and nuclear fission heated TFEs (partially adapted from Ref. 48).

Characterization

Some internal, unmeasurable characteristics of a thermionic converter or a TFE, which are extremely important for assessing any performance degradation during operation and for on-line performance optimization, can be inferred from measurable parameters. For example, considering any two points (1 and 2) on two static (constant thermal input power to the emitter) voltampere characteristics (Fig. 14), the difference in the total heat removal from the emitter at the same

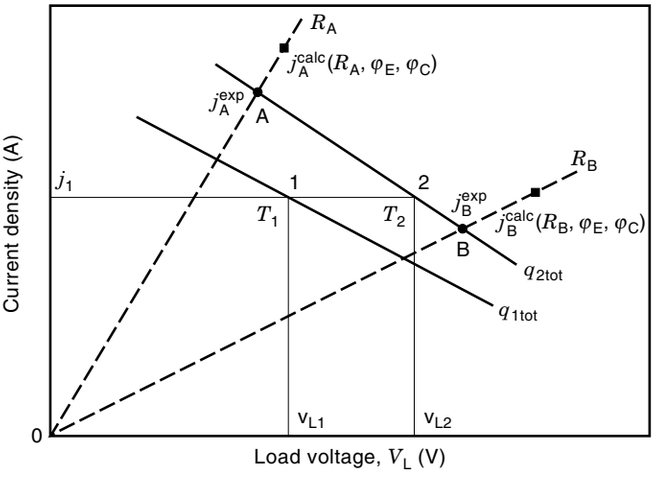

Figure 14. A schematic for determining the effective emissivity and work functions of the electrodes.

current density, j_1, can be written as

$$q_{2\text{tot}} - q_{1\text{tot}} = (q_{\text{rad2}} - q_{\text{rad1}}) + j_1(V_{\text{L2}} - V_{\text{L1}}) + \frac{2k}{e}(T_2 - T_1)j_1 + (q_{\text{Cs2}} - q_{\text{Cs1}}) + (q_{\text{str2}} - q_{\text{str1}}) - 0.5(q_{\text{J2}} - q_{\text{J1}}) \quad (22)$$

In this equation, the subscripts rad, Cs, str, and J refer to radiation heat transfer, conduction heat transfer in the Cs-filled interelectrode gap, end heat losses in the electrodes, and joule heating, respectively. When the total input power, $q_{2\text{tot}}$, is slightly higher than $q_{1\text{tot}}$, the collector temperatures at points 1 and 2 are approximately equal and the effective emissivity of electrodes, ϵ, can readily be determined. The two power levels, $q_{1\text{tot}}$ and $q_{2\text{tot}}$, should be close enough, however, so that the corresponding collector temperatures can be assumed almost the same. Therefore, the calculated effective emissivity corresponds to the average emitter temperature at points 1 and 2 in Fig. 14. Equation (22) can thus be used to calculate the effective emissivity of the interelectrode gap at different combinations of T_1 and T_2 and determine its dependence on the average emitter temperature, for system performance analyses during testing and operation lifetime. To apply Eq. (22), however, the contributions of heat conduction through the interelectrode gap and end losses through the electrodes should be calculated using, for example, Eqs. (16) and (18a), respectively.

The effective work functions of the electrodes can then be estimated on the basis of the experimental voltampere characteristics, assuming linear characteristics, which is typically the case in ignited mode discharge, within a certain range of load voltages, using the reverse solution of Eqs. (13) and (22). In this approach, the electrode temperatures, the cesiated work functions, and the gap size are related to the measured load current and voltage. Assuming linear voltampere characteristics, load resistance (R_A and R_B), and corresponding current densities (j_A and j_B), the cesiated work functions are found from the following equalities:

$$j_A^{\text{exp}} = j^{\text{calc}}(R_A, \varphi_E, \varphi_C) \quad (23a)$$

$$j_B^{\text{exp}} = j^{\text{calc}}(R_B, \varphi_E, \varphi_C) \quad (23b)$$

In these equations, j^{exp} and j^{calc} are the experimental and calculated current densities (at points A and B in Fig. 14), respectively. Solving Eqs. (23a) and (23b) for the different electrode temperatures and different cesium pressures, dependencies of the electrodes' effective work functions on the emitter and collector temperature as well as the vapor pressure can be obtained based on actual, on-line measurements of the voltampere characteristics. The determined values can then be compared with initial values of the electrodes' work functions to determine any changes as a function of operation lifetime.

APPLICATION TO SPACE ELECTRIC POWER GENERATION

Historically, the interest in thermionic conversion technology has been driven by its potential use in nuclear reactor space power systems. In these systems, the nuclear reactor serves as the heat source and could be coupled with the thermionic conversion elements, either in an in-core or ex-core arrangement. In the former, the thermionic fuel elements (for example, see Fig. 6) are arranged typically in a compact, triangular lattice. The nuclear fuel pellets are staked inside the emitter tubes of the TFEs. The heat generated from nuclear fission is then transferred by radial conduction through the fuel pellets (typically UO_2, 90 wt% enriched), to the emitter tubes of the TFEs (typically at 1800 K to 1900 K). The heat transferred to the collector assembly (Fig. 6) is then removed by circulating a liquid-metal coolant (typically NaK or Na).

In the ex-core arrangements, the TICs are placed outside the nuclear reactor core, and heat is transported, typically using Na heat pipes, to the inside of the emitter tubes. The heat from the collector assembly of the TFEs is removed either by a circulating liquid-metal coolant or by heat pipes and rejected to space by thermal radiation through the radiator assembly. The heat rejection radiator of a thermionic space nuclear reactor system is typically the most voluminous and massive component of the system. The ex-core arrangement has the advantage of a compact nuclear reactor core, which means smaller reactor mass and smaller size and mass of the shadow radiation shield. The disadvantage, compared to the in-core arrangements, however, is that the reactor coolant has to operate at very high temperatures, requiring using high-temperature refractory alloys as the structure material. On the other hand, in the in-core arrangement the highest temperature in the system is limited to the fuel stack and the emitter tube. The rest of the system operates at or below the collector temperature, typically 800 K to 1000 K, hence allowing using stainless steel as the structure material for the rest of the system. More details of the design of thermionic space nuclear power systems could be found elsewhere (49–61).

APPLICATION TO TERRESTRIAL SPACE ELECTRIC POWER GENERATION

The interest in using thermionic conversion in a number of commercial and military terrestrial applications began as early as the 1960s (62,63). The high emitter temperature of thermionic converters makes them attractive for use in topping cycles of terrestrial fossil fuel power plants, where high temperatures exist in combustion chambers (64). Thermionic conversion had been considered for a topping cycle for various types of gas and steam turbine power plants (65–67) and cogeneration plants (68–70). The idea of implementing a thermionic topping cycle is simple: Hot gases in the combustion chamber heat the emitter of thermionic converters up to ~1600 K to 2000 K to achieve satisfactory thermionic performance. The collector is cooled (~800 K to 900 K) with forced air flow before entering the combustion chamber (Fig. 15).

The work performed in the early 1980s under the Department of Energy's (DOE) thermionic technology program demonstrated that using a thermionic topping cycle in a gas turbine power plant could increase the plant's overall efficiency and the electric power by several percentage points (67,72). In 1984, when this program reached the demonstration stage, the DOE suggested that the US industry take over the financing of the terrestrial thermionics, but industry was not yet ready to invest in this type of advanced electric power generation.

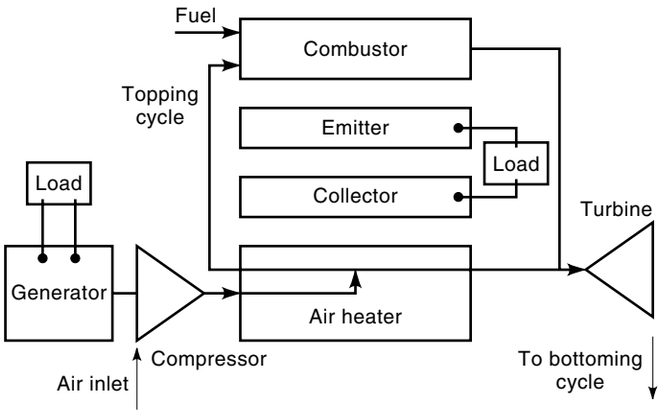

Figure 15. A schematic of thermionic converter being used in the topping cycle of a gas turbine, electric power generation plant (71).

Recent advances in natural-gas-fired gas turbines, such as integrated gasification combined cycle (IGCC) and pressurized fluidized bed combustion (PFBC) technologies, have made using a thermionic topping cycle that employs state-of-the-art or near-term advanced TI technology even less attractive. Recent studies of using thermionic topping cycles have shown that, even using advanced thermionic technology (for example, microgap converters), the efficiency of combined cycle power plants that employ advanced GTs, such as Westinghouse 501ATS, can be increased only by less than 1.5 percentage points (71). Such a small performance gain does not justify using a thermionic topping cycle, considering the technology development required and the risks involved. As far as using a TI topping cycle in coal-fired steam power plants, the relatively low efficiency of thermionic converters makes these far less competitive with IGCC and PFBC gas turbine electric power generation plants.

One of the most recent advancements in the field of terrestrial thermionics has been made by the Dutch-Russian joint venture ECS (73,74). A number of natural-gas-fired cogeneration devices, ranging from a small domestic cogeneration unit to a large industrial burner, have been designed. The program culminated in manufacturing and testing a thermionic module heated by a natural-gas-fired recuperative burner. The ECS thermionic converter has a CVD silicon carbide protective coating, but the collector is water cooled. The emitter area is 38 cm^2 and the interelectrode gap is 0.4 mm to 0.5 mm wide. This converter produced a maximum electric power output of 69 W ($\sim$1.8 W/cm^2) while operating at an emitter temperature (T_E) of only 1623 K. For an assembly consisting of 12 cylindrical thermionic converters having emitter surface area of 38 W/cm^2 each and operating at T_E = 1600 K, an electrical power output of 625 W ($\sim$1.37 W/cm^2) and overall conversion efficiency of 8.4% were projected (75).

For more than a decade, Space Power Inc. (SPI), in cooperation with Scientific-Industrial Association "Luch" of Russia, has been developing combustion-heated microgap thermionic converters with active gap control for cogeneration applications. A conversion efficiency of about 13% at an emitter temperature of 1300 K is projected. Other potential terrestrial applications of thermionic conversion include automotive waste heat recovery (76) and high-temperature solar power systems in remote areas.

BIBLIOGRAPHY

1. C. Herring and M. H. Nichols, Thermionic emission, *Rev. Mod. Phys.,* **21**: 185–270, 1949.
2. G. N. Hastopoulos, The thermoelectron engine, Sc.D. dissertation, MIT, Cambridge, MA, 1956.
3. F. G. Baksht et al., *Thermionic Converters and Low-Temperature Plasma,* Rep. No. DOE-tr-1, Washington, DC: U.S. Dept. Energy, Tech. Inf. Center, 1978.
4. J. M. Houston, Theoretical performance of the thermionic energy conversion, *J. Appl. Phys.,* **30** (4): 1959.
5. V. C. Wilson, Conversion of heat to electricity by thermionic emission, *J. Appl. Phys.,* **30**: 475, 1959.
6. K. P. Luke, Thermionic work function of a single crystal, Sc.D. thesis, MIT, Cambridge, MA, 1964.
7. V. S. Fomenko, in G. V. Samsonov (ed. and trans.), *Handbook of Thermionic Properties,* New York: Plenum, 1966.
8. D. Steiner and E. P. Gystopoulos, An equation for the prediction of the bare work functions, *Proc. 27th Annu. Conf. Phys. Electron.,* Cambridge, MA, 1967, pp. 160–168.
9. G. N. Hastopoulos and F. Rufeh, Thermodynamic correlation of work function, *Energy Convers.,* **10**: 135, 1970.
10. G. N. Hastopoulos and E. P. Gystopoulos, On the relation between work function and other thermophysical properties, *Proc. Thermionic Convers. Spec. Conf.,* Miami Beach, FL, 1970, pp. 203–209.
11. T. Alleau and M. Bacal, Influence of oxygen adsorption and oxygen-cesium coadsorption on (100) tungsten work function, *Proc. Thermionic Convers. Spec. Conf.,* Miami Beach, FL, 1970, pp. 434–440.
12. J.-L. Denisot, *Electron Emission Experimental Study of a (100) Tungsten Single Crystal Covered wtih Cesium and Oxygen,* CEA-R-4508, France; Commissariat à l'Energie Atomique, 1973.
13. N. S. Rasor, Thermionic energy conversion, *Appl. At. Collission Phys.,* **5**: 170–220, 1982.
14. M. S. El-Genk, H. Xue, and C. Murray, Transient and load-following characteristics of a fully integrated single-cell thermionic fuel element, *J. Nucl. Technol.,* **102**: 145–166, 1993.
15. W. R. Wilkins and E. P. Gyftopoulos, Transport phenomena in low energy plasmas, *J. Appl. Phys.,* **37**: 3533–3540, 1966.
16. D. W. Culp, *Principle of Energy Conversion,* New York: McGraw-Hill, 1997.
17. S. Kitrilakis and M. Meeker, Experimental determination of the heat conduction of cesium gas, *Adv. Energy Convers.,* **3**: 59–68, 1963.
18. G. N. Hastopoulos and E. P. Gyftopoulos, *Thermionic Energy Conversion,* Vol. 1, Cambridge, MA: MIT Press, 1973.
19. V. A. Korykin, V. P. Obrezumov, and V. I. Vybyvanets, Variation of emission-adsorption properties in an operating TEC collector, *Proc. 24th IECEC,* Vol. 2, 1989, pp. 1161–1164.
20. C. B. Geller et al., *Final Report of the High Efficiency Thermionics (HET-IV) and Converter Advancement (CAP) Programs,* Rep. No. WAPD-T-3106, West Mifflin, PA: Bettis Atomic Power Laboratory, Westinghouse Electric Corp., 1996.
21. J. L. Desplat, W (100) work function change during adsorption of oxygen, cesium, and oxygen-cesium co-adsorption, *Proc. 3rd Int. Conf. Thermionic Electr. Power Generation,* Juelich, Germany, 1972, pp. 1397–1407.
22. B. Gunther et al., *Summary Report on Oxygen Additives,* Rep. TEF-3056-2. Thermo Electron Corp., 1974.
23. D. V. Paramonov and M. S. El-Genk, An analysis of emitter material transport in thermionic converters, *AIP Conf. Proc.,* **361** (3): 1137–1148, 1996.

24. D. V. Paramonov and M. S. El-Genk, Effect of oxygen on the operation of a single-cell thermionic fuel element, *J. Nucl. Mater.,* **256**: 218–228, 1998.
25. V. I. Babanin et al., Optimization of a Knudsen Cs-Ba thermionic converter, *Sov. Phys.—Tech. Phys.,* **23**: 444–451, 1978.
26. Yu. K. Szhenov, A. F. Piskunov, and V. A. Osadchii, *Teplofiz. Vys. Temp.,* **10**: 738, 1972.
27. V. I. Babanin et al., Potential distribution in a two-gas thermionic converter at current saturation, *Sov. Phys.—Tech. Phys.,* **17**: 1695–1700, 1973.
28. A. Y. Ender et al., Ultra-high temperature thermionic system for space solar power application, *AIP Conf. Proc.,* **301**: 861–867, 1994.
29. V. M. Gun'ko and P. V. Smirnova, High temperature oxidation of tungsten in presence of cesium vapor, *J. Phys. Chem.,* **57**: 2581–2583, 1983.
30. V. A. Korykin and V. P. Oberzumov, Dynamics of changes in thermionic energy converter collector properties under conditions of mass transfer in the interelectrode gap, *Proc. 25th IECEC,* 1990, pp. 332–339.
31. D. V. Paramonov and M. S. El-Genk, An analysis of Ya-21 thermionic fuel elements test results, *AIP Conf. Proc.,* **361**: 1395–1400, 1996.
32. M. S. El-Genk and J. Luke, Performance comparison of thermionic converters with smooth and micro-grooved electrodes, *J. Energy Convers. Manage.,* **39**: 1–13, 1998.
33. M. S. El-Genk and Y. Momozaki, Performance evaluation of a thermionic converter with a macro-grooved emitter and a smooth collector, *AIP Conf. Proc.,* **420**: 308–316, 1998.
34. K. Shimada, Low arc drop hybrid mode thermionic converter, *Proc. 12th Intersoc. Energy Convers. Eng. Conf. (IECEC),* Soc. Automot. Eng., 1977, pp. 1568–1574.
35. K. Shimada, Recent progress in hybrid mode thermionic converter development, *Proc. 14th Intersoc. Energy Convers. Eng. Conf. (IECEC),* 1979, pp. 1890–1893.
36. V. K. Tskhakaya, L. P. Chechelashvili, and V. I. Yarygin, Hybrid operating mode of a thermionic converter with a grooved collector, *Sov. Phys.—Tech. Phys.,* **28**: 869–870, 1983.
37. V. D. Atamasov et al., Experimental study of cesium arc thermionic converters with multicavity anodes, *Sov. Phys.—Tech. Phys.,* **29**: 42–45, 1984.
38. C. Lee, D. Lieb, and G. Miskolczy, Ceramic composites for thermionic fuel elements, *Proc. 25th IECEC,* 1990, pp. 294–299.
39. D. V. Paramonov and M. S. El-Genk, A review of cesium thermionic converters with developed emitter surfaces, *J. Energy Convers. Manage.,* **38**: 533–549, 1996.
40. C. Kaplan and J. B. Merzenich, *Proc. Thermionic Convers. Spec. Conf.,* Cleveland, OH, 1966, p. 333.
41. E. S. Bekmukhambetov et al., Cesium thermionic converter with additives of the inert gases, *Sov. J. Tech. Phys.,* **96**: 1481–1482, 1966 (in Russian).
42. F. V. Kondrat'ev, G. V. Sinyutin, and V. F. Tikhonov, Effect of xenon addition on the operation of a cesium thermionic converter, Atomnaya Energiya, **23**:208, 1967.
43. F. Rufeh and S. S. Kitrilakis, *Proc. Thermionic Convers. Spec. Conf.,* Houston, TX, 1996.
44. I. G. Gverdtsiteli et al., *Proc. 2nd Int. Conf. Thermionic Elect. Power Generation,* Stresa, Italy, 1968, p. 1097.
45. F. Rufeh and D. Lieb, The influence of inert gases on the I-V characteristics of a cesium diode, *J. Energy Convers.,* **10**: 149–153, 1970.
46. R. Ya. Kucherov et al., *J. Sov. Phys.—Tech. Phys.,* **15**: 1937, 1971.
47. K. G. Tschersich and E. A. Niekizch, Xenon induced changes of the I-V curves of a thermionic converter, *Proc. IECEC,* 1975, pp. 376–381.

47a. G. Fitzpatrick et al., Demonstration of close-spaced thermionic converters, *Proc. 28th IECEC,* American Chemical Society, 1.573–1.580, 1993.

47b. G. Fitzpatrick et al., Close-spaced thermionic converter with small gap, *AIP Conf. Proc. 361,* M. S. El-Genk (ed.), 1299–1304, 1996.

48. V. V. Sinyavskii et al., *Design and Testing of Thermionic Fuel Elements,* Moscow: Atomizolet, 1981 (in Russian).
49. N. Rasor and R. C. Howard, Nuclear thermionic space power systems, *Proc. 18th Annu. IAS Propulsion Meet.,* Inst. Aerosp. Sci., Cleveland, OH, 1963.
50. W. J. Leovic and C. Z. Kamien, Solar thermionic power systems development, *Prog. Astronaut. Aeronaut.,* **6**: 1966.
51. C. D. Sawyer, P. R. Hill, and D. R. Wilkins, Multimegawatt thermionic reactor systems for space applications, *Proc. 2nd Int. Conf. Thermionic Electr. Power Generation,* Stresa, Italy, 1968, pp. 171–184.
52. J. J. Ward, R. Breitwieser, and R. M. Williams, Conceptual design of a 150 Kwe out-of-core nuclear thermionic converter system, *Proc. 9th Annu. Thermionic Conf. Spec. Meet.,* Miami Beach, FL, 1970, pp. 179–184.
53. Gulf General Atomic Co., *Development of a Thermionic Space Power System,* Final Summ. Rep. (Gulf GA-A126o8), San Diego, CA: Gulf Atomics, 1973.
54. G. M. Gryaznov et al., Thermionic reactors-converters for space NPS, *At. Energ.,* **66** (6): 374, 1989.
55. N. G. Gunther, *Characteristics of the Soviet TOPAZ II Space Power Systems,* Rep. SPI-52-1, San Jose, CA: Space Power Inc., 1990.
56. J. G. Jacox et al., Small ex-core heat pipe thermionic reactor concept (SEHPTR). *Proc. 25th IECEC,* Monterey, CA, 1990.
57. J. C. Mills et al., A fast spectrum heat pipe cooled thermionic power system, *AIP Conf. Proc.,* **246**: 504–509, 1992.
58. T. H. Van Hagan and B. R. Lewis, TFE fast driver reactor system for low-power applications, *AIP Conf. Proc.* **246**: 498–503, 1992.
59. H. S. Rhee et al., Space-R thermionic space nuclear power system with single cell incore thermionic fuel element, *AIP Conf. Proc.,* **246**: 120–129, 1992.
60. W. R. Determan and T. H. Van Hagan, Space power reactor incore thermionic multicell evolutionary (S-PRIME) design, *AIP Conf. Proc.,* **271**: 1235–1239, 1993.
61. M. S. El-Genk, *A Critical Review of Space Nuclear Power and Propulsion 1984–1993,* New York: American Institute of Physics, 1994.
62. L. J. Lazaridis, P. G. Pantazelos, and I. Shai, *Design of a Gas-Fired Thermionic Power Supply for Domestic Furnaces,* Paper No. 66-WA/ENER-3, New York: ASME, 1966.
63. L. J. Lazaridis and P. G. Pantazelos, Test of flame-heated thermionic diode, *Proc. 10th Annu. Power Sources Conf.,* Atlantic City, NJ, 1966.
64. F. Huffman, Overview of terrestrial thermionics, *Proc. 18th IECEC,* Paper No. 839027, 1983, pp. 179–185.
65. G. O. Fitzpatrick, E. J. Britt, and G. Carnasciali, Increased central station power plant efficiency with a thermionic topping system, *Proc. 12th IECEC,* 1977, pp. 1602–1609.
66. G. Miscolczy, G. Gunter, and A. E. Margulies, Conceptual design of a thermionic topped steam electric generator plant, *Proc. 13th IECEC,* 1978, pp. 1893–1897.
67. G. Miscolczy et al., Thermionic combustor application to combined gas and steam turbine power plants, *Proc. 16th IECEC,* 1981, pp. 1956–1961.

68. G. Miscolczy and D. Lieb, Cogeneration using a thermionic combustor, *Proc. 17th IECEC,* 1982, pp. 1918–1923.
69. G. Miscolczy et al., Cogeneration burner module design, *Proc. 18th IECEC,* 1983, pp. 186–191.
70. R. S. Dick, Thermionic cogeneration burner assessment, *Proc. 19th IECEC,* 1984, pp. 2307–2312.
71. D. V. Paramonov and M. D. Carelli, A thermionic topping cycle for advanced gas turbines, *Proc. 33rd IECEC,* American Nuclear Society, Chicago, 1998.
72. G. O. Fitzpatrick et al., Thermionic converters for increased performance in gas turbine power plants, *Proc. 16th IECEC,* 1981, pp. 1962–1967.
73. L. R. Wolff, Small scale thermionic cogeneration systems: Commercialization perspectives, *Proc. Thermionic Energy Convers. Spec. Conf.,* Goteborg, Sweden, 1993, pp. 57–63.
74. V. I. Yarygin et al., Combustion heated cold seal TEC, *Proc. 32nd Intersoc. Energy Convers. Eng. Conf. (IECEC),* 1997, pp. 2264–2270.
75. V. I. Yarygin et al., Test of a TEC-module, *Proc. 29th Intersoc. Energy Convers. Eng. Conf. (IECEC),* 1994, pp. 1061–1066.
76. R. Svenson and L. Holmid, TEC as electric generator in an automobile catalytic converter, *Proc. 31st IECEC,* IEEE, 1996, pp. 941–944.

MOHAMED S. EL-GENK
University of New Mexico
DMITRY V. PARAMONOV
Westinghouse Science and
Technology Center